www.nature.com/aps

Acta Pharmacologica Sinica

ARTICLE

Loss of DJ-1 function contributes to Parkinson's disease pathogenesis in mice *via* RACK1-mediated PKC activation and MAO-B upregulation

Le-le Liu[1], Yu Han[1], Zi-jia Zhang[2], Yi-qi Wang[1], Yu-wei Hu[1], Elena Kaznacheyeva[3], Jian-qing Ding[4], Dong-kai Guo[5], Guang-hui Wang[1], Bin Li[6]✉ and Hai-gang Ren[1]✉

Parkinson's disease (PD) is a common neurodegenerative motor disorder characterized by a dramatic reduction in pars compacta of substantia nigra dopaminergic neurons and striatal dopamine (DA) levels. Mutations or deletions in the *PARK7/DJ-1* gene are associated with an early-onset familial form of PD. DJ-1 protein prevents neurodegeneration via its regulation of oxidative stress and mitochondrial function as well as its roles in transcription and signal transduction. In this study, we investigated how loss of DJ-1 function affected DA degradation, ROS generation and mitochondrial dysfunction in neuronal cells. We showed that loss of DJ-1 significantly increased the expression of monoamine oxidase (MAO)-B but not MAO-A in both neuronal cells and primary astrocytes. In *DJ-1*-knockout (KO) mice, MAO-B protein levels in the substantia nigra (SN) and striatal regions were significantly increased. We demonstrated that the induction of MAO-B expression by DJ-1 deficiency depended on early growth response 1 (EGR1) in N2a cells. By coimmunoprecipitation omics analysis, we found that DJ-1 interacted with receptor of activated protein C kinase 1 (RACK1), a scaffolding protein, and thus inhibited the activity of the PKC/JNK/AP-1/EGR1 cascade. The PKC inhibitor sotrastaurin or the JNK inhibitor SP600125 completely inhibited DJ-1 deficiency-induced EGR1 and MAO-B expression in N2a cells. Moreover, the MAO-B inhibitor rasagiline inhibited mitochondrial ROS generation and rescued neuronal cell death caused by DJ-1 deficiency, especially in response to MPTP stimulation in vitro and in vivo. These results suggest that DJ-1 exerts neuroprotective effects by inhibiting the expression of MAO-B distributed at the mitochondrial outer membrane, which mediates DA degradation, ROS generation and mitochondrial dysfunction. This study reveals a mechanistic link between DJ-1 and MAO-B expression and contributes to understanding the crosslinks among pathogenic factors, mitochondrial dysfunction and oxidative stress in PD pathogenesis.

Keywords: Parkinson's disease; DJ-1; MAO-B; EGR1; RACK1; PKC

Acta Pharmacologica Sinica (2023) 44:1948–1961; https://doi.org/10.1038/s41401-023-01104-8

INTRODUCTION

Parkinson's disease (PD) is the most common age-related neurodegenerative movement disorder and affects ~1% of people over 65 years old and ~5% of people at age 85. In PD, pars compacta of substantia nigra (SNpc) dopaminergic neurons and striatal dopamine (DA) levels are dramatically diminished [1]. Clinical symptoms of PD include motor disorders such as bradykinesia, rigidity, postural instability and resting tremor as well as nonmotor symptoms such as dementia, depression and autonomic dysfunction [2, 3], all of which seriously reduce the quality of life of patients. Because the pathogenesis of PD is still unclear, DA supplements such as levodopa (*L*-DOPA) are still the mainstays of PD treatment but are accompanied by many adverse reactions [4–6].

Both environmental toxins and genetic factors contribute to PD pathogenesis. There is strong evidence that impaired mitochondrial function and oxidative stress are key pathological factors in PD [7]. The most well-known PD inducer, 1-methyl-4-phenyl-1, 2, 3,6-tetrahydropyridine (MPTP), is converted to 1-methyl-4-phenylpyridinium (MPP^+) by monoamine oxidase (MAO)-B, which selectively damages DA neurons mainly by inhibiting mitochondrial complex I function and inducing reactive oxygen species (ROS), leading to parkinsonism in human and animal models [8]. Other neurotoxins, such as 6-hydroxydopamine (6-OHDA), paraquat and rotenone, also induce DA neuron loss by impairing mitochondrial function and leading to ROS production [8]. Moreover, many PD-associated genetic factors, such as *SCNA*, *PRKN*, *PINK1*, and *PARK7*, also have essential roles in mitochondrial function and oxidative stress [9].

Mutations in DJ-1/PARK7, including L166P, are associated with an early-onset familial form of PD [10]. In addition, decreased

[1]Laboratory of Molecular Neuropathology, Jiangsu Key Laboratory of Translational Research and Therapy for Neuropsychiatric Disorders & Department of Pharmacology, College of Pharmaceutical Sciences, Soochow University, Suzhou 215123, China; [2]Qingdao Municipal Hospital of Shandong Province, Qingdao 266011, China; [3]Institute of Cytology, Russian Academy of Sciences, Saint-Petersburg 194064, Russia; [4]Department of Neurology and Institute of Neurology, Ruijin Hospital Affiliated to Shanghai Jiaotong University School of Medicine, Shanghai 200025, China; [5]Laboratory of Clinical Pharmacy, Suzhou Hospital, Affiliated Hospital of Medical School, Nanjing University, Suzhou 215153, China and [6]Department of General Surgery, Suzhou Ninth Hospital Affiliated to Soochow University, Suzhou 215200, China
Correspondence: Bin Li (bli4004@suda.edu.cn) or Hai-gang Ren (rhg@suda.edu.cn)
These authors contributed equally: Le-le Liu, Yu Han, Zi-jia Zhang

Received: 5 January 2023 Accepted: 1 May 2023
Published online: 25 May 2023

levels of DJ-1 mRNA and protein have been found in sporadic PD brains compared with age-matched individuals [11]. The highly conserved and widely expressed DJ-1 protein has been demonstrated to prevent neurodegeneration via its regulation of oxidative stress and mitochondrial function as well as its roles in transcription and signal transduction. DJ-1 inhibits ROS production and protects cells against various oxidative agents, such as DA, H_2O_2, 6-OHDA and MPTP; in contrast, DJ-1 deficiency sensitizes cell death to these oxidative neurotoxins [12]. Recent evidence suggests that deletion of DJ-1 leads to impaired DA metabolism. Patients harboring DJ-1 mutants show presynaptic DA deficits [13, 14]. Several laboratory groups, including our team, have demonstrated that DJ-1 positively regulates tyrosine hydroxylase (TH) expression [15–18]. More importantly, oxidized DA and mitochondrial oxidative stress are dramatically increased in differentiated homozygous DJ-1 mutant DA neurons from PD patients who harbor homozygous loss-of-function mutations in *DJ-1* compared with healthy controls [19]. Notably, reduced DA synthesis is insufficient to explain these abnormal pathological changes caused by the loss of DJ-1 function. Therefore, we speculated that loss of DJ-1 function may disturb DA degradation, which contributes to mitochondrial dysfunction, oxidative stress and neurodegeneration.

Impaired DA metabolism resulting in DA decline, excessive ROS generation and subsequent events is crucial for PD pathogenesis [20, 21]. Mitochondrial-localized MAOs catalyze the oxidative deamination of monoamines, including DA, leading to DA degradation and ROS generation; these events contribute to activation of the death signal pathway, and MAO-mediated DA metabolism dysfunction plays essential roles in PD pathogenesis [20, 22, 23]. MAOs are present in most tissues in the form of two isoenzymes, MAO-A and MAO-B, which are encoded by separate genes and share ~70% identity [24]. Both MAO-A and MAO-B are localized at the mitochondrial outer membrane, with predominant distribution in glial cells and DA neurons as well as other neuronal populations with distinct distributions in specific brain regions [22, 25, 26].

Here, we found that DJ-1 deficiency increased MAO-B but not MAO-A expression in vitro and in vivo. Induction of MAO-B expression by DJ-1 deficiency was dependent on early growth response 1 (EGR1) expression. Binding to receptor of activated protein C kinase 1 (RACK1) and regulation of the activity of protein kinase C (PKC) were involved in DJ-1-mediated MAO-B expression. DJ-1 deficiency led to PKC activation followed by c-JUN N-terminal kinase (JNK) and c-JUN activation, which subsequently induced EGR1 and MAO-B expression. In addition, the PKC inhibitor sotrastaurin or the JNK inhibitor SP600125 inhibited EGR1 and MAO-B expression induced by DJ-1 deficiency. Moreover, the MAO-B inhibitor rasagiline (Rasa) inhibited mitochondrial ROS production and neuronal cell death caused by loss of DJ-1, especially in response to neurotoxic stimulation in vitro and in vivo.

MATERIALS AND METHODS

Animals

DJ-1-KO mice were kindly provided by Dr. Jie Shen of Harvard Medical School [27]. Male mice were used in this study. For immunoblotting, DA measurement and MAO-B activity assays, 12-month-old *DJ-1*-KO mice and littermate wild-type mice were sacrificed to isolate substantia nigra (SN) and striatal tissue samples. For immunochemistry, the mice were perfused with 4% paraformaldehyde after 0.9% saline perfusion. Then, the mouse brains were removed and postfixed with 4% paraformaldehyde overnight before being incubated with 30% sucrose solution overnight at 4 °C. Serial slices of midbrains with a thickness of 20 μm were cut with a frozen microtome (Leica, German). For behavioral tests, 10–12-month-old *DJ-1*-KO mice and wild-type mice were used. All mice were used according to the institutional guidelines for animal use and care, and all procedures were approved by the ethical committee of Soochow University.

Reagents

DA, the PKC inhibitor sotrastaurin and the MAO-B inhibitor Rasa were purchased from Selleckchem (Houston, USA). Phorbol 12-myristate 13-acetate (PMA) was purchased from Sigma (St. Louis, MO, USA). The JNK inhibitor SP600125 was purchased from Beyotime Biotechnology (Nantong, China).

Drug administration in mice

The procedure for drug administration in mice is shown in Fig. 8e. Ten- to 12-month-old *DJ-1*-KO mice and control mice were randomly divided into three groups: the vehicle group, the MPTP group, and the Rasa + MPTP group. Beginning 3 days before MPTP treatment, mice were given Rasa at a dose of 3 $mg{\cdot}kg^{-1}{\cdot}d^{-1}$ or an equal volume of water intragastrically for 18 consecutive days. Then, mice were intraperitoneally injected with MPTP for 7 consecutive days (25 $mg{\cdot}kg^{-1}{\cdot}d^{-1}$ in the first 3 days and 30 $mg{\cdot}/kg^{-1}{\cdot}d^{-1}$ in the last 4 days), while the control group was given an equal volume of PBS. The behavioral tests were performed beginning on Day 13. On the 18th day, all mice were sacrificed for immunochemistry.

Plasmids

p3xFLAG-DJ-1, p3xFLAG-DJ-1^{L166P}, DJ-1-MYC or DJ-1^{L166P}-MYC have been described previously [28, 29]. A 0.4 kb fragment of the murine *MAO-B* promoter (nucleotides −314 to +91) was amplified from a mouse genomic DNA library with the primers 5′-CGACGCGTGAAAGGCTCTTAATCTTTGG-3′ and 5′-CCCTCGAGGCTG CTTGCTAGGTTCCA-3′ and inserted into the PGL3-Basic vector at *MluI*/*Xho*I sites. A mutated *MAO-B* promoter that lacks the EGR1 binding site (Δ-116/-91) was generated by site-directed mutagenesis using the PGL3-*MAO-B*-luciferase plasmid as a template with the primers 5′-AGGGTTAAGAGCTCCACCCAG-3′ and 5′-AGCCCGAC AACACAGGCACAAG-3′. pJSX-GL3 (murine *c-JUN* luciferase) (Addgene plasmid #11980) and 3xAP1pGL3 (*3xAP-1 RE* in pGL3-basic) (Addgene plasmid #40342) containing three canonical AP-1 binding sites (TGACTCA) were gifts from Ron Prywes [30] and Alexander Dent [31], respectively. pcDNA3.1-EGR1 was purchased from YouBio (Changsha, China). The fidelities of all constructs were confirmed by sequencing.

Cell culture and plasmid transfection

Mouse neuroblastoma Neuro2a (N2a) cells, human neuroblastoma SH-SY5Y cells and human embryonic kidney 293 (HEK293) cells were grown in Dulbecco's modified Eagle's medium (DMEM, Gibco, Grand Island, NY, USA) containing 10% fetal bovine serum (FBS, Gibco) with streptomycin (100 μg/mL) and penicillin (100 U/mL) (Gibco). For plasmid transfection, cells were transfected with plasmids using Lipofectamine 2000 transfection reagent (Invitrogen, Carlsbad, CA, USA) according to the manufacturer's instructions.

Primary astrocyte culture

Primary cultured astrocytes were cultured as described elsewhere [32]. In brief, the cortex tissues of newborn C57BL/6 mice were chopped and dissected. After being digested with 0.25% trypsin (Gibco) at 37 °C for 15 min, the isolated cells were plated on poly-*D*-lysine-coated 24-well plates (Corning, Tewksbury, MA, USA) and cultured in DMEM/F12 containing penicillin (100 mg/mL), streptomycin (100 mg/mL) and 10% heat-inactivated FBS for 14 days. The culture medium was replaced every 3 days. After separating microglia from mixed glial cells by shaking at 150 rpm for 2 h at 37 °C, the primary astrocytes were cultured for further experiments.

Small interfering RNA (siRNA) knockdown

siRNAs against the mouse *DJ-1* gene were synthesized with the following sequences: *DJ-1* 1#: 5′-CGCUUGUUCUCAAAGACUATT-3′ and 5′-UAGUCUUUGAGAACAAGCGGT-3′; *DJ-1* 2#: 5′-GGCUCUG UUGGCUCACGAATT-3′ and 5′-UUCGUGAGCCAACAGAGCCGT-3′; siRNAs against the human *DJ-1* gene were synthesized with the following sequences: 5′-UGGAGACGGUCAUCCCUGUTT-3′ and 5′-ACAGGGAUGACCGUCUCCATT-3′. Cells were transfected with siRNAs using Lipofectamine RNAiMAX transfection reagent (Invitrogen) according to the manufacturer's instructions.

Transcriptome sequencing

First, total RNA was extracted using TRIzol reagent (Invitrogen) from three technical repeats. Quality control and library construction were entrusted to Huada Gene Technology Company, and then transcriptome sequencing was performed using the BGISEQ platform. The raw data were filtered to remove reads of low quality, reads with adaptor sequences and reads with high levels of N bases. The clean reads were aligned to the reference genome using HISAT software. KEGG pathway enrichment was performed, differentially expressed genes (DEGs) were identified and expression analysis was conducted on the Dr. Tom analysis system (https://biosys.bgi.com).

Quantitative real-time PCR (qRT–PCR)

The procedures for RNA extraction and reverse transcription have been described elsewhere [33]. qRT–PCR analysis was performed for quantitative measurement of the target RNA abundance with Power SYBR Green PCR Master Mix (Applied Biosystems, Foster City, CA, USA) using a 7500 Real-Time PCR system (Applied Biosystems). The mouse primer sequences used for real-time PCR were as follows: 5′-AGCCGGGATCAAAGTCACTG-3′ and 5′-GGTCC CTGCGTTTTTGCATC-3′ for *DJ-1*; 5′-GAGGCTCCAATTTCAATCACT CTG-3′ and 5′-ATGTAGTTTAGCAAGTCGTTCAGC-3′ for *MAO-A*; 5′-AAGCGATGTGATCGTGGTGG-3′ and 5′-ACACTGAGGCCACAATC ATGC-3′ for *MAO-B*; 5′-TGACGCAAAAGGCCAAATCAT-3′ and 5′-CCA TTCGCACGGCTGAGTAG-3′ for *COMT*; 5′- TAGCTGACTATCTGGATG GCAT-3′ and 5′-GTCCTCGTATGTTTCTGGCTC-3′ for *DDC*; 5′-GCCGA GCGAACAACCCTAT-3′ and 5′-TCCACCATCGCCTTCTCATT-3′ for *EGR1*; 5′-GCCAACCTCAGCAACTTCAAC-3′ and 5′-GGAAGAGCCGCA GACCGT-3′ for *c-JUN*; 5′-GGGGAGAAGCCTTTTACCTG-3′ and 5′-AGC CTGGGATCTTCTTGGTT-3′ for *Tieg2*; and 5′-GCTACAGCTTCACCAC CACA-3′ and 5′-TCTCCAGGGAGGAAGAGGAT-3′ for *β-actin* as an internal control. Relative gene expression was calculated by the $2^{-\Delta\Delta CT}$ method.

Luciferase reporter assay

N2a cells were cotransfected with luciferase reporter and expression plasmids along with the Renilla luciferase vector pRL-CMV as an internal control for normalization. The total amount of plasmid DNA was held constant by the addition of empty plasmid. Cell extracts were prepared with Passive Lysis Buffer (Promega) 48 h after transfection, and the luciferase activity was measured with a dual luciferase assay kit (Promega) using an Infinite M1000 Pro microplate reader (Tecan, Austria GmbH, Groedig, Austria) according to the manufacturer's instructions.

Immunoblot analysis

Cell extracts were lysed in cell lysis buffer (50 mM Tris-HCl pH 7.5 buffer containing 150 mM NaCl, 1% NP40, 0.5% deoxycholate and the protease inhibitor cocktail (Roche)). Approximately 20 μg of protein was electrophoresed and electrotransferred to a polyvinylidene difluoride membrane (PVDF, Millipore, Billerica, MA, USA). The blots were incubated with the following primary antibodies: rabbit polyclonal anti-DJ-1 (AB9212, Millipore), anti-EGR1 (sc-110, Santa Cruz, CA, USA), anti-ERK1/2 (sc-93, Santa Cruz), anti-MYC (sc-789, Santa Cruz), anti-c-JUN (10024-2-AP, Proteintech, Rosemont, USA), anti-phospho-c-JUN (Ser73) (D155011, Sangon Biotech, Shanghai, China), anti-PKCβ (12919-1-AP, Proteintech), anti-phospho-PKCβ (#9371, Cell Signaling Danvers, MA, USA), anti-RACK1 (sc-17754, Santa Cruz), anti-PARP (#9532, Cell Signaling) and anti-cleaved Caspase-3 (#9661, Cell Signaling) antibodies; rabbit monoclonal anti-MAO-A (ab126751, Abcam, Cambridge, UK), anti-MAO-B (ab125010, Abcam), anti-MAO-B (12602-1-AP, Proteintech) and anti-phospho-JNK1/2/3 (Y185/Y185/Y223) (ab76572, Abcam) antibodies; and mouse monoclonal anti-DJ-1 (sc-55573, Santa Cruz), anti-JNK (sc-7345, Santa Cruz), anti-phospho-ERK1/2 (sc-7383, Santa Cruz), anti-GAPDH (MAB374, Millipore) antibodies. The following secondary antibodies were used: horseradish peroxidase-conjugated sheep anti-mouse and anti-rabbit antibodies (Amersham Pharmacia Biotech, Piscataway, NJ, Sweden). The proteins were visualized with an ECL detection kit (Thermo Fisher, Waltham, MA, USA) using a chemiluminescence imaging system (Bioshine ChemiQ 4800, Shanghai, China).

Immunoprecipitation (IP)

Cells were lysed in cell lysis buffer at 4 °C. After centrifugation at 12,000 × *g* for 15 min, the supernatants were used for IP with appropriate antibodies coupled to protein G Sepharose beads (Roche, Basel, Basel-City, Switzerland). The immunoprecipitates were then washed with cell lysis buffer and subjected to immunoblot analysis. The input represents 10% of the supernatant used in the co-IP experiments. To screen DJ-1 binding partners, the supernatants of SH-SY5Y or HEK293 cells transfected with FLAG or FLAG-DJ-1 were subjected to IP with an anti-FLAG antibody, and the immunoprecipitates were analyzed with mass spectrometry by Huada Gene Technology Company.

Immunofluorescence (IF) and immunohistochemistry (IHC)

For IF, cells were washed with PBS (Gibco, pH 7.4) and fixed with 4% paraformaldehyde for 5 min. After being permeabilized with 0.25% Triton X-100 in PBS, the cells were washed with PBS 3 times and preblocked with 4% fetal bovine serum for 1 h in PBST (0.1% Tween 20 in PBS). Then, the cells were incubated with the indicated antibodies overnight before incubation with fluorescent secondary antibodies (Alexa Fluor 594-conjugated and 488-conjugated AffiniPure donkey anti-rabbit or anti-mouse antibodies, Invitrogen) for 2 h. The cells were then labeled with DAPI for 10 min. For IHC, serial slices from mouse midbrains were stained overnight with anti-TH antibodies (AB152, Millipore) and then incubated with Alexa Fluor 594-conjugated AffiniPure donkey anti-rabbit antibodies for 2 h. Then, the slices were labeled with 4′,6-diamidino-2-phenylindole (DAPI, Sigma) for 10 min. The labeled cells or slides were visualized using an AIR HD25 confocal microscope (Nikon, Japan).

Mitochondrial ROS measurement

Mitochondrial ROS production was monitored using MitoSOX™ Red (Invitrogen), a red mitochondrial superoxide indicator that exhibits red fluorescence when oxidized by superoxide in the mitochondria. Briefly, SH-SY5Y cells were incubated for 20 min at 37 °C with 2.5 μM MitoSOX and 10 μM Hoechst 33258 diluted in HBSS and then washed twice. MitoSOX fluorescence was visualized using a TIE2 inverted microscope system (Nikon, Japan).

DA measurement

The DA concentration was measured using high-performance liquid chromatography (HPLC) according to the methods in our previous study [15]. Briefly, the weighed striatum of each mouse was homogenized with 0.4 M perchloric acid by ultrasound on ice for 5 s. After centrifugation, the supernatants were filtered with 0.22 μm membranes, and 20 μl of each sample was injected into the HPLC (ANTEC, Netherlands) for DA analysis. The levels of DA in the striatum were quantified by calculating the peak area of the standard product (Sigma) with various concentration gradients.

Behavioral experiments

Mouse training and behavioral tests were performed according to our previous study [34]. For the rotarod test, on training days, all mice were trained by placing them on the rotarod until they were able to remain on the rotarod for more than 2 min at a speed of 4 rpm. On the test days, mice were placed on the rotarod (SANS Biological Technology, Nanjing, China), and the speed was slowly accelerated from 4 rpm to 40 rpm within 5 min. The latency to the first fall of each mouse was recorded. The test was repeated three times for each mouse. For the pole test, a rough-surfaced wood pole (SANS Biological Technology) with a length of 50 cm and a diameter of 1 cm was used. On training days, all mice were trained three times by placing them on the top of the pole and allowing them to crawl downward from top to the home cage. On the test days, the time it took for each mouse to climb down the pole was recorded. The test was repeated three times for each mouse, and the average time was analyzed.

MAO-B activity assay

MAO-B activity was measured using an MAO Activity Kit (ab241031, Abcam) according to the manufacturer's instructions. Briefly, the cell or tissue samples were homogenized with assay buffer and centrifuged, and the supernatants were collected. Then, an MAO-A inhibitor (clorgyline, 10 μM) was added to the supernatant, and the samples were incubated for 10 min at 25 °C. Then, MAO Reaction Mix was added, and the fluorescence (Ex/Em = 535/587 nm) was measured in kinetic mode at 25 °C for 60 min.

MTT cell viability assay

Cells were washed with PBS and incubated with MTT (3-(4,5)-dimethylthiazol(-2-y1)-2,5-di-phenyltetrazolium bromide, Sigma, St. Louis, MO, USA) (0.5 mg/mL) dissolved in DMEM without phenol red. After 3 h, the medium was removed, and the formazan crystals were dissolved in DMSO (dimethyl sulfoxide) by incubating at 37 °C for 30 min. The absorbance was measured by a photometer at 570 nm by subtracting the background at 630 nm. The data were normalized to a control, and the ratios are presented as the means ± SD from three independent experiments.

Statistical analysis

Densitometric analysis of immunoblots from three independent experiments was performed using Photoshop 7.0 software (Adobe, San Jose, CA, USA). The data from at least three independent experiments were analyzed with GraphPad Prism 8.0 software (San Diego, CA, USA). Statistical analysis was performed by one-way analysis of variance (ANOVA) or two-way ANOVA. Student's *t* tests were used to compare two groups. A *P* value of <0.05 was considered to indicate statistical significance. All results are presented as the mean ± SD.

RESULTS

MAO-B but not MAO-A expression is upregulated by DJ-1 deficiency

To explore the roles of DJ-1 loss in DA neuronal cells, we used two murine *DJ-1*-targeted siRNAs to silence DJ-1 expression in cultured N2a cells and screened the DEGs affected by DJ-1 deficiency by transcriptome sequencing. Both *DJ-1*-targeting siRNAs significantly decreased *DJ-1* expression levels according to transcriptome sequencing (Fig. 1a). We found that the expression levels of 122 genes were changed in both *DJ-1*-knockdown groups compared to the control group under the criteria of at least a 1.5-fold change (FC) and a *P* value of <0.05 (Fig. 1a). Interestingly, we found that the tyrosine metabolic pathway was significantly enriched among these 122 genes through KEGG pathway analysis (Fig. 1b). Among them, the genes involved in the tyrosine metabolic pathway were *MAO-B*, *TH* and DA β-hydroxylase (*DBH*), and the clustering heatmaps of these three DEGs indicated that the expression of *MAO-B* was increased in *DJ-1*-knockdown cells, while that of *DBH* and *TH* was decreased (Fig. 1c). The mechanism by which DJ-1 regulates *TH* has been elucidated [15–18]. DBH catalyzes DA to form norepinephrine, and its deficiency mainly affects the sympathetic nervous system [35]. Therefore, in the present study, we focused on whether and how DJ-1 regulates MAO-B expression.

To verify whether DJ-1 affects MAO-B expression, we performed qRT–PCR to measure the mRNA levels of MAO-B and other DA metabolic enzymes. We found that *DJ-1*-targeting siRNA-mediated *DJ-1* knockdown significantly increased *MAO-B* mRNA levels without affecting *MAO-A*, DOPA decarboxylase (*DDC*) or catechol-O-methyltransferase (*COMT*) (Fig. 2a). We further detected whether MAO-B protein levels were affected by DJ-1 knockdown. As shown in Fig. 2b and c, both *DJ-1*-targeted siRNAs significantly increased the protein levels of MAO-B without obvious changes in those of MAO-A. Interestingly, we also found that MAO-B but not MAO-A expression was upregulated by DJ-1 silencing in primary astrocytes which plays an important role in DA degradation (Fig. 2d and e). We also examined the effect of DJ-1 on MAO expression in SH-SY5Y cells, a human neuroblastoma cell line. Knockdown of DJ-1 in SH-SY5Y cells also significantly upregulated MAO-B expression but not MAO-A expression (Fig. 2f and g). Correspondingly, we found that knockdown of DJ-1 significantly increased MAO-B activity (Fig. 2h). We next examined whether loss of DJ-1 influenced MAO-B expression in vivo. We isolated the SN and striatal regions of mouse brains and found that MAO-B protein levels were significantly increased in both the SN and striatum in *DJ-1*-KO mice compared with the littermate controls (Fig. 2i and j). We also examined MAO-B activity in wild-type and *DJ-1*-KO mice. As shown in Fig. 2k, MAO-B activity was significantly increased in the SN of *DJ-1*-KO mice. Together, these results revealed that DJ-1 deficiency specifically activates *MAO-B* but not *MAO-A* transcription in cultured neuronal cells and primary astrocytes as well as in vivo.

The regulation of MAO-B expression by DJ-1 is EGR1 dependent

We next investigated which transcription factors are responsible for the regulation of *MAO-B* transcription by DJ-1. Considering that *MAO-B*, but not *MAO-A*, is transcriptionally activated upon loss of DJ-1, we focused on the transcription factors that specifically activate *MAO-B* transcription. The core regions of the *MAO-A* and *MAO-B* promoters are GC-rich and share ~60% sequence identity, and they are transcriptionally regulated by several common transcription factors. They also each contain a unique organization of cis-response elements and are differentially regulated by several distinct transcription factors, among which early growth response protein 1 (EGR1) is specifically responsible for *MAO-B* transcription [36]. EGR1 specifically activates *MAO-B* gene expression but not *MAO-A* expression by binding to EGR1-binding motifs (5′-GCG(T/G)GGGCG-3′) in the *MAO-B* promoter [37–39]. We analyzed the human and mouse *MAO-B* promoter sequences and found that there is an EGR1 binding motif within nucleotides −89 to −81 in the human *MAO-B* promoter and triple overlapping EGR1 binding sites within nucleotides −111 to −91 in the mouse *Mao-b* promoter (Fig. 3a). To examine whether EGR1 participates in the regulation of MAO-B transcription by DJ-1, we cloned the 0.4 kb core regions of the mouse *MAO-B* promoter containing triple overlapping EGR1 binding motifs (wt-*MAO-B*-Luc) and a mutant *MAO-B* promoter lacking EGR1 binding motifs (nucleotides −116 to −91) (m-*MAO-B*-Luc) into a luciferase reporter vector (Fig. 3b). Overexpression of EGR1 dramatically increased wild-type *MAO-B* promoter activity (Fig. 3c). Moreover, the activity of the mutant *MAO-B* promoter lacking the EGR1 binding sites was dramatically reduced compared to that of the wild-type *MAO-B* promoter, and overexpression of EGR1 no longer had an activating

a

	Log_2FC	*P*-value
si-*DJ-1* 1#	-5.43	0
si-*DJ-1* 2#	-4.27	0

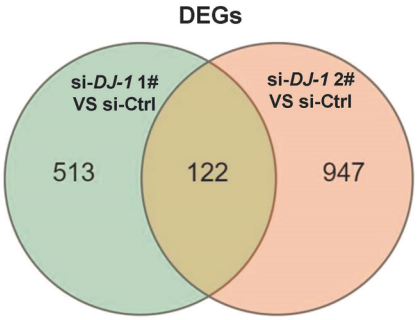

b

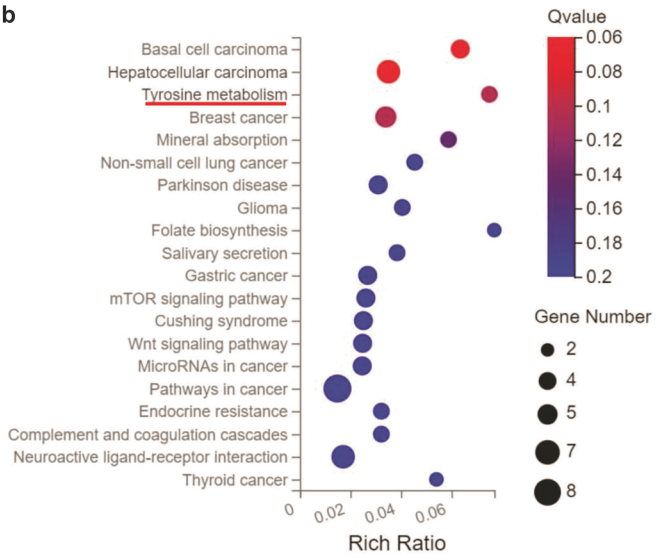

c

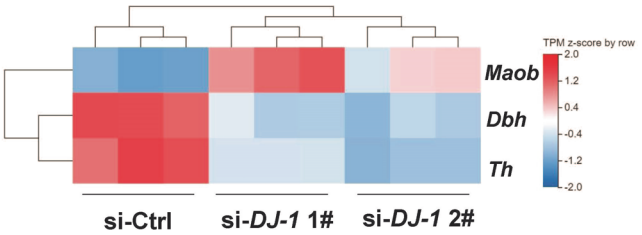

Fig. 1 DJ-1 deficiency affects DA metabolic gene expression according to RNAseq. a Silencing efficiency of two *DJ-1*-knockdown groups compared to the control group (si-Ctrl) according to transcriptome sequencing and a Venn diagram representation of the number of DEGs identified in each individual and in both (fold change ≥ 1.5, $P < 0.05$). **b** KEGG pathway analyses of 122 DEGs in (**a**). **c** Heatmap of the transcripts per million (TPM) values of genes involved in tyrosine metabolism in each group.

effect on the mutant *MAO-B* promoter activity (Fig. 3c). In addition, overexpression of EGR1 in N2a cells significantly increased MAO-B protein levels rather than MAO-A protein levels (Fig. 3d and e). These results suggest that EGR1 is a major and specific transcription factor for MAO-B expression. We next examined whether DJ-1 and its PD pathogenic L166P mutant regulated *MAO-B* promoter activity. As shown in Fig. 3f, overexpression of FLAG-DJ-1 significantly repressed wild-type *MAO-B* promoter activity; however, overexpression of the L166P mutant, which is considered a loss-of-DJ-1-function mutant [40], had no inhibitory effect on *MAO-B* promoter activity. In addition, FLAG-DJ-1 lost its inhibitory effect on the activity of the mutant *MAO-B* promoter lacking the EGR1 binding sites (Fig. 3g). These results indicate that the repression of *MAO-B* transcription by DJ-1 is EGR1 dependent.

EGR1 expression is activated by DJ-1 deficiency

We next examined how DJ-1 regulates EGR1-mediated MAO-B expression. We first detected whether EGR1 expression is affected by DJ-1 silencing. As shown in Fig. 4a and b, both *DJ-1*-targeting siRNAs dramatically increased EGR1 protein levels. We also found that the mRNA levels of *EGR1* were significantly increased in DJ-1-knockdown cells, but not those of *Tieg2*, a gene whose product KLF11 transcriptionally activates both *MAO-B* and *MAO-A* [41, 42] (Fig. 4c). This result also explained why DJ-1 specifically regulated MAO-B expression rather than MAO-A expression. We also examined the effect of DJ-1 on EGR1 expression in SH-SY5Y cells. As shown in Fig. 4d and e, knockdown of DJ-1 significantly increased EGR1 protein levels in SH-SY5Y cells. Together, these results suggest that loss of DJ-1 function activates MAO-B expression by inducing EGR1 expression.

AP-1 is responsible for DJ-1 deficiency-induced EGR1 and MAO-B expression

EGR1 expression has been reported to be activated by several mitogen-activated protein kinases (MAPKs) [43–46]. DJ-1 has been shown to regulate the activity of these MAPKs in cancer cells or neuronal cells [12]. Therefore, we examined whether DJ-1 deficiency affects MAPK activity in neuronal cells. Interestingly, knockdown of DJ-1 significantly increased JNK1/2/3 and p38 phosphorylation but slightly decreased ERK1/2 activity (Fig. 5a and b). As extracellular signal-regulated kinase (ERK) and c-JUN N-terminal kinases (JNKs), rather than p38, have been reported to activate EGR1 expression [43–46], the decreased ERK1/2 activation and increased p38 activation caused by DJ-1 deletion may not contribute to EGR1 induction by DJ-1 deficiency. Therefore, we focused on whether DJ-1 deficiency induces the expression of EGR1 and MAO-B by activating the JNK pathway. Interestingly, SP600125, a JNK-specific inhibitor, completely blocked DJ-1 deficiency-induced MAO-B and EGR1 upregulation in N2a cells (Fig. 5c and d). These results suggested that loss of DJ-1 function activates EGR1 and MAO-B expression by activating the JNK pathway.

c-JUN is a major component of the heterodimeric transcription factor AP-1. Both c-JUN and AP-1 activities are activated by JNK-mediated phosphorylation at Ser63 and Ser73 within the c-JUN N-terminus and subsequently activate transcription of target genes such as *EGR1* and *c-JUN* itself [47–49]. Therefore, we measured whether DJ-1 deletion affects the phosphorylation of c-JUN at Ser73 as well as c-JUN protein levels. c-JUN phosphorylation at Ser73 and c-JUN protein levels were dramatically increased in *DJ-1*-silenced cells (Fig. 5e and f).

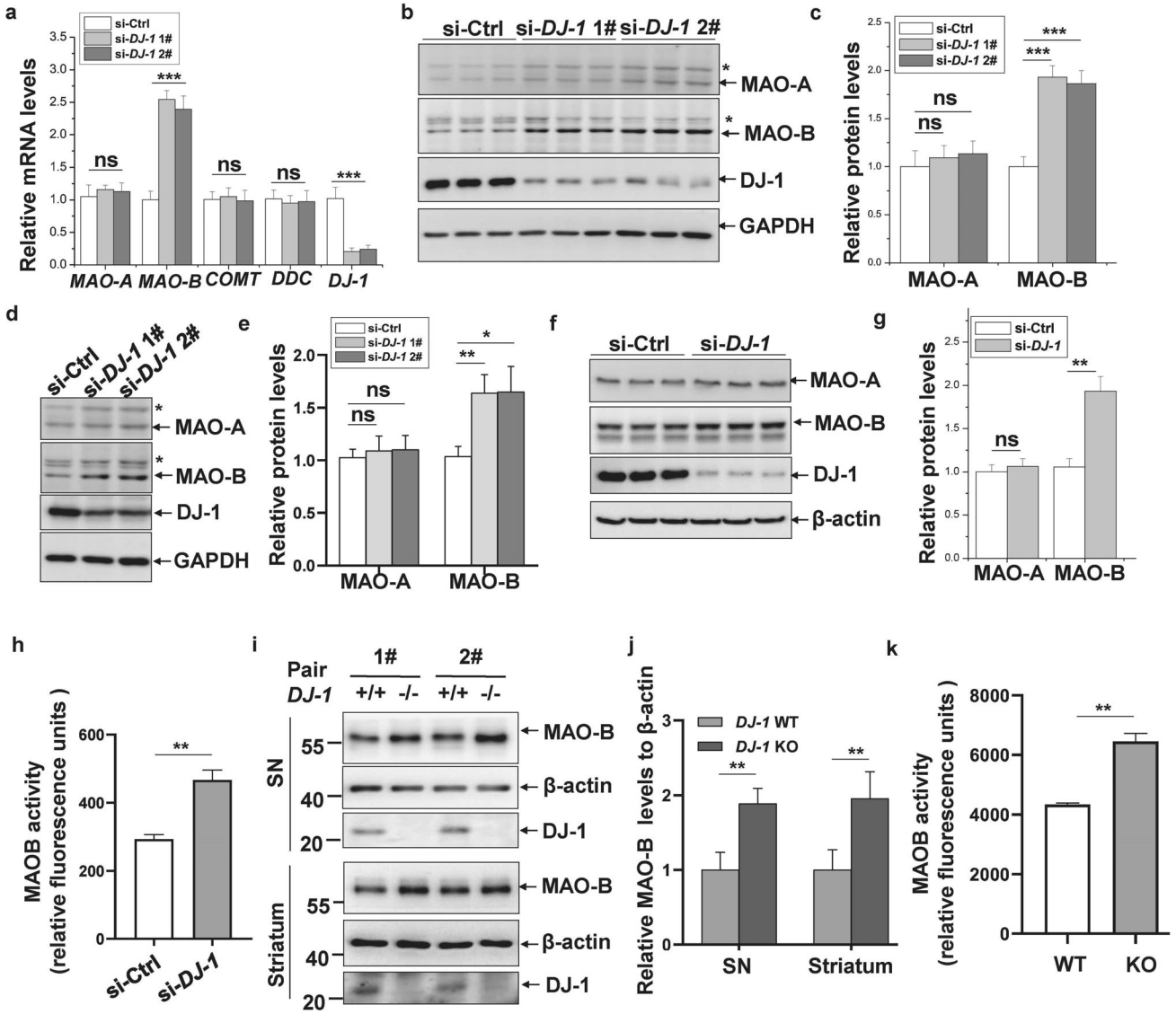

Fig. 2 MAO-B but not MAO-A expression is upregulated by DJ-1 deficiency. a N2a cells were transfected with the indicated siRNAs. Seventy-two hours after transfection, qRT–PCR was performed. ***, $P < 0.001$, ns, no statistical significance, $n = 4$. **b** N2a cells were transfected with the indicated siRNAs. Seventy-two hours after transfection, the cell lysates were subjected to immunoblot analysis. *, unspecific bands. **c** The relative protein levels of MAO-A or MAO-B to GAPDH in (**b**) were analyzed. ***, $P < 0.001$, ns, no statistical significance, $n = 3$. **d** Primary astrocytes were transfected with the indicated siRNAs. Seventy-two hours after transfection, the cell lysates were subjected to immunoblot analysis. *, unspecific bands. **e** The relative protein levels of MAO-A or MAO-B to GAPDH in (**d**) were analyzed. **, $P < 0.01$, *, $P < 0.05$, ns, no statistical significance, $n = 3$. **f** SH-SY5Y cells were transfected with the indicated siRNAs. Seventy-two hours after transfection, the cell lysates were subjected to immunoblot analysis. **g** The relative protein levels of MAO-A or MAO-B to β-actin in (**f**) were analyzed. **, $P < 0.01$, ns, no statistical significance, $n = 3$. **h** SH-SY5Y cells were transfected with the indicated siRNAs. Seventy-two hours after transfection, MAO-B activity was measured. **, $P < 0.01$, $n = 3$. **i** MAO-B protein levels in the SN and striatum of *DJ-1*-KO mice and littermate controls were subjected to immunoblot analysis. **j** The relative protein levels of MAO-B to β-actin in (**h**) were analyzed. **, $P < 0.01$, $n = 4$. **k** MAO-B activity was measured in the SNs of *DJ-1*-KO mice and littermate controls. **, $P < 0.01$, $n = 4$.

c-JUN mRNA levels were also dramatically increased in *DJ-1*-silenced cells (Fig. 5g). *c-JUN* promoter activity was also significantly inhibited by overexpression of FLAG-DJ-1 (Fig. 5h). We also examined whether AP-1 transcriptional activity is affected by DJ-1 using a *3xAP-1* response element (RE) luciferase plasmid containing three canonical AP-1 binding sites. Overexpression of FLAG-DJ-1 significantly inhibited AP-1 transcriptional activity (Fig. 5i). Together, these results suggest that loss of DJ-1 activates EGR1 and MAO-B expression by activating the JNK pathway and inducing AP-1 transcriptional activity and that blocking JNK activity can completely inhibit MAO-B induction caused by DJ-1 deficiency.

Wild-type DJ-1, but not the L166P mutant, interacts with RACK1

To further explore the mechanism by which DJ-1 regulates JNK activity and EGR1 and MAO-B expression, we performed IP followed by mass spectrometry (IP-MS) to screen DJ-1 binding partners. We performed IP-MS using an anti-FLAG antibody from cell lysates of SH-SY5Y and HEK293T cells transfected with FLAG or FLAG-DJ-1. As shown in Fig. 6a, compared with the FLAG control, FLAG-DJ-1 pulled 260 and 392 specific proteins down from SH-SY5Y and HEK293T cells, respectively, of which 94 proteins were detected in both types of cells. Among these 94 proteins, we focused on receptor for activated C kinase 1 (RACK1) (Fig. 6b). RACK1 is well known as an adaptor for protein kinase C (PKC)-

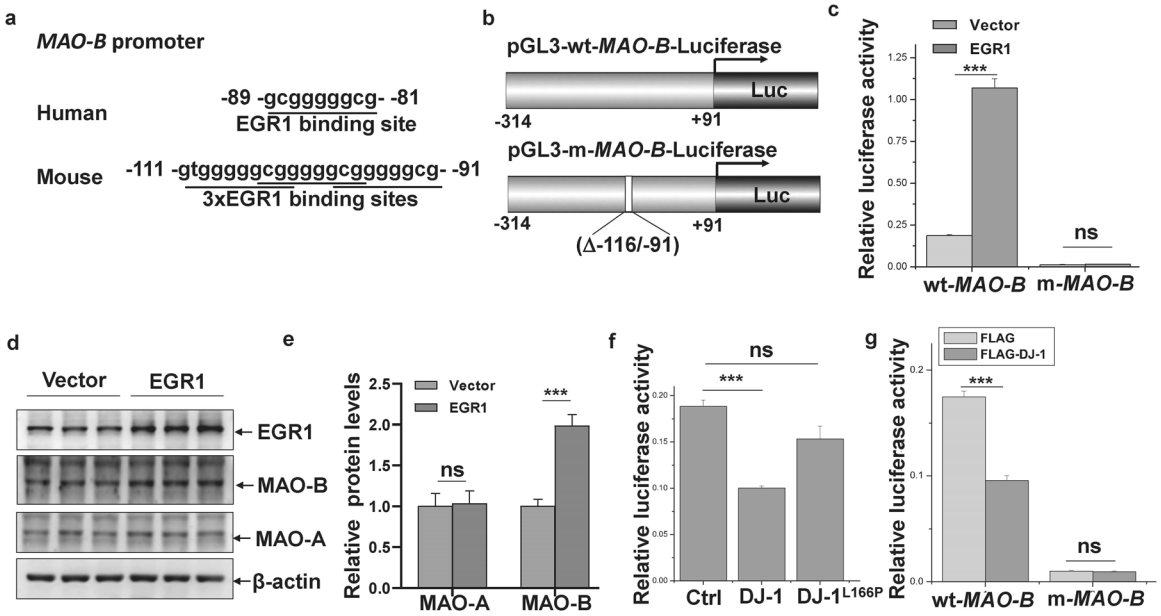

Fig. 3 The regulation of MAO-B expression by DJ-1 is EGR1 dependent. a Both human and mouse *MAO-B* promoters contain EGR1 binding motifs. **b** Schematic representation of the wild-type (wt) *MAO-B* promoter and mutant (m) *MAO-B* promoter that lacks EGR1 binding motifs constructed in the PGL3-Basic vector. **c** N2a cells were transfected with PGL3-wt-*MAO-B*-Luc or PGL3-m-*MAO-B*-Luc along with pcDNA3.1 or pcDNA3.1-EGR1. Forty-eight hours after transfection, luciferase reporter assays were performed. ***, $P < 0.001$, ns, no statistical significance, $n = 4$. **d** N2a cells were transfected with pcDNA3.1 or pcDNA3.1-EGR1. Forty-eight hours after transfection, the cell lysates were subjected to immunoblot analysis. **e** The relative protein levels of MAO-A or MAO-B to GAPDH in (**d**) were analyzed. ***, $P < 0.001$, ns, no statistical significance, $n = 3$. **f** N2a cells were transfected with PGL3-wt-*MAO-B*-Luc along with FLAG, FLAG-DJ-1 or FLAG-DJ-1^{L166P}. Forty-eight hours after transfection, luciferase reporter assays were performed. ***, $P < 0.001$, ns, no statistical significance, $n = 4$. **g** N2a cells were transfected with PGL3-wt-*MAO-B*-Luc or PGL3-m-*MAO-B*-Luc along with FLAG or FLAG-DJ-1. Forty-eight hours after transfection, luciferase reporter assays were performed. ***, $P < 0.001$, ns, no statistical significance, $n = 4$.

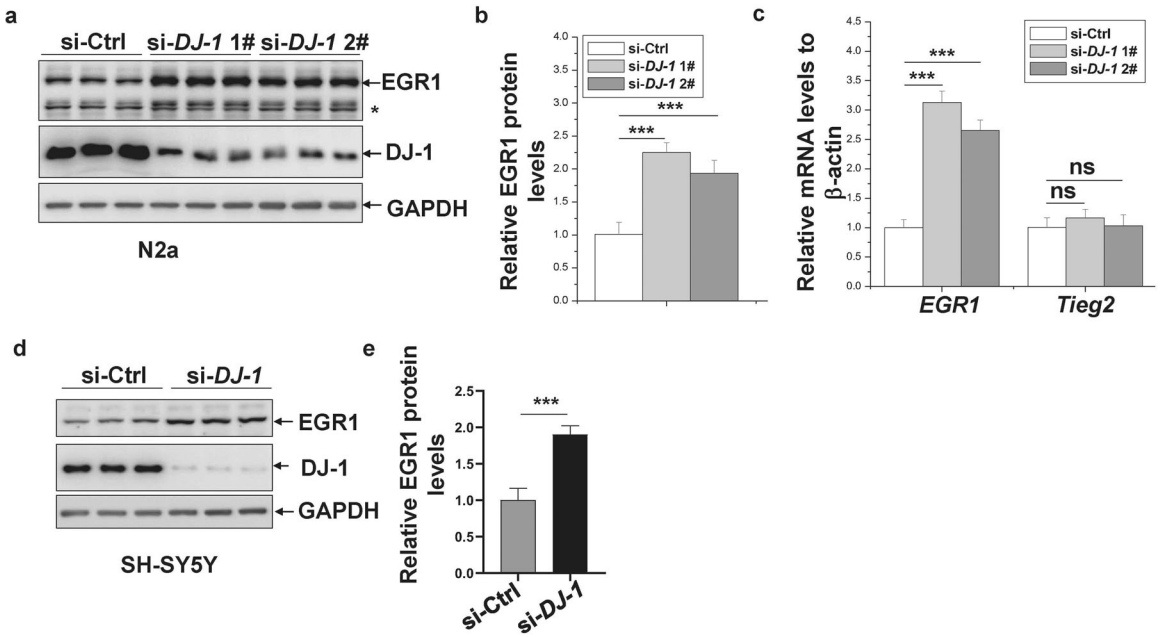

Fig. 4 EGR1 expression is activated by DJ-1 deficiency. a N2a cells were transfected with the indicated siRNAs. Seventy-two hours after transfection, the cell lysates were subjected to immunoblot analysis. *, unspecific bands. **b** The relative levels of EGR1 to GAPDH in (**a**) were analyzed. ***, $P < 0.001$, $n = 3$. **c** N2a cells were transfected with the indicated siRNAs. Seventy-two hours after transfection, qRT–PCR was performed. ***, $P < 0.001$, ns, no statistical significance, $n = 4$. **d** SH-SY5Y cells were transfected with the indicated siRNAs. Seventy-two hours after transfection, the cell lysates were subjected to immunoblot analysis. **e** The relative levels of EGR1 to GAPDH in (**d**) were analyzed. ***, $P < 0.001$, $n = 3$.

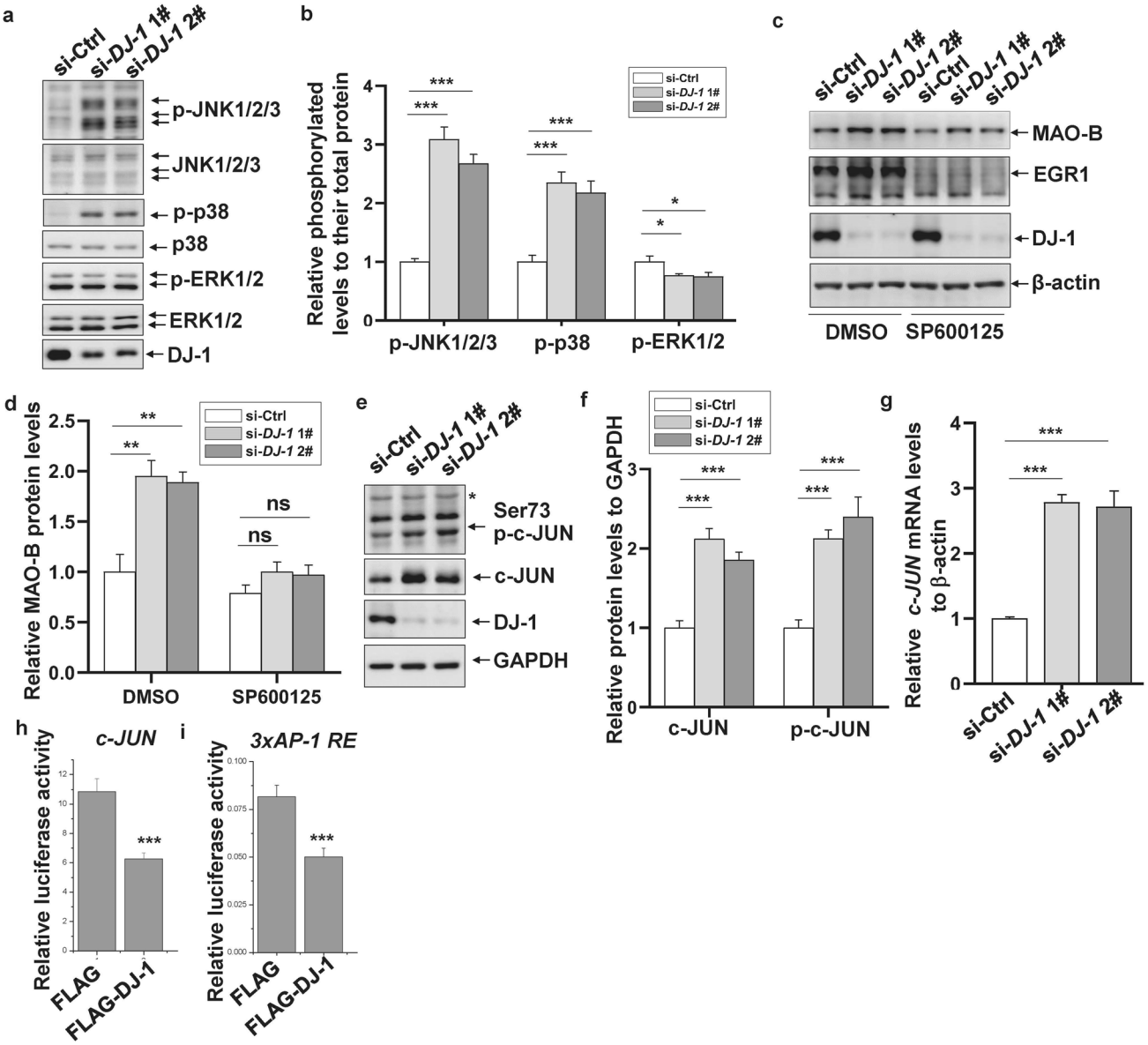

Fig. 5 AP-1 is responsible for DJ-1 deficiency-induced EGR1 and MAO-B expression. N2a cells were transfected with the indicated siRNAs. Seventy-two hours after transfection, the cell lysates were subjected to immunoblot analysis. **b** The relative levels of p-JNK, p-p38 or p-ERK1/2 to GAPDH in (**a**) were analyzed. ***, $P < 0.001$, *, $P < 0.05$, $n = 3$. **c** N2a cells were transfected with the indicated siRNAs. Twenty-four hours after transfection, cells were treated with 10 μM SP600125 for 48 h, and then the cell lysates were subjected to immunoblot analysis. **d** The relative protein levels of MAO-B and EGR1 to GAPDH in (**c**) were analyzed. **, $P < 0.01$, ns, no statistical significance, $n = 3$. **e** N2a cells were transfected with the indicated siRNAs. Seventy-two hours after transfection, the cell lysates were subjected to immunoblot analysis. *, unspecific bands. **f** The relative protein levels of c-JUN or p-c-JUN to GAPDH in (**e**) were analyzed. ***, $P < 0.001$, $n = 3$. **g** N2a cells were transfected with the indicated siRNAs. Seventy-two hours after transfection, qRT–PCR was performed. ***, $P < 0.001$, $n = 4$. **h–i** N2a cells were transfected with pJSX-GL3-Luc (**h**) or 3xAP1pGL3-Luc (**i**) along with FLAG or FLAG-DJ-1. Forty-eight hours after transfection, luciferase reporter assays were performed. ***, $P < 0.001$, $n = 4$.

mediated full JNK activation, and PKC signaling is essential for MAO-B expression [37, 50–52]. We verified the interaction of FLAG-DJ-1 with RACK1 through IP using an anti-FLAG antibody in SH-SY5Y cells (Fig. 6c). We also examined whether DJ-1 binds to the transcription factors involved in MAO-B expression, such as EGR1 and the AP-1 complex (c-JUN and c-FOS), and found that DJ-1 did not bind to them (Fig. 6c). We further confirmed this interaction between endogenous DJ-1 and RACK1 through IP using anti-RACK1 or anti-DJ-1 antibodies (Fig. 6d and e), and immunofluorescence showed strong colocalization of DJ-1 and RACK1 in the cytoplasm (Fig. 6f). We also tested whether the DJ-1^{L166P} mutant interacts with RACK1. Due to the rapid degradation of DJ-1^{L166P} through the proteasome [53], triple the amount of the FLAG-DJ-1^{L166P} construct compared to FLAG-DJ-1 was used in the transfection to obtain a level of expression comparable to that of FLAG-DJ-1. Interestingly, unlike FLAG-DJ-1, FLAG-DJ-1^{L166P} was almost unable to pull down RACK1 (Fig. 6g), suggesting that the L166P mutant lacked the ability to bind to RACK1. We also found that the fluorescence of wild-type DJ-1 but not DJ-1^{L166P} was colocalized with RACK1 in cells (Fig. 6h). These results suggest that wild-type DJ-1, but not the pathogenic L166P mutant, interacts with RACK1 in the cytoplasm.

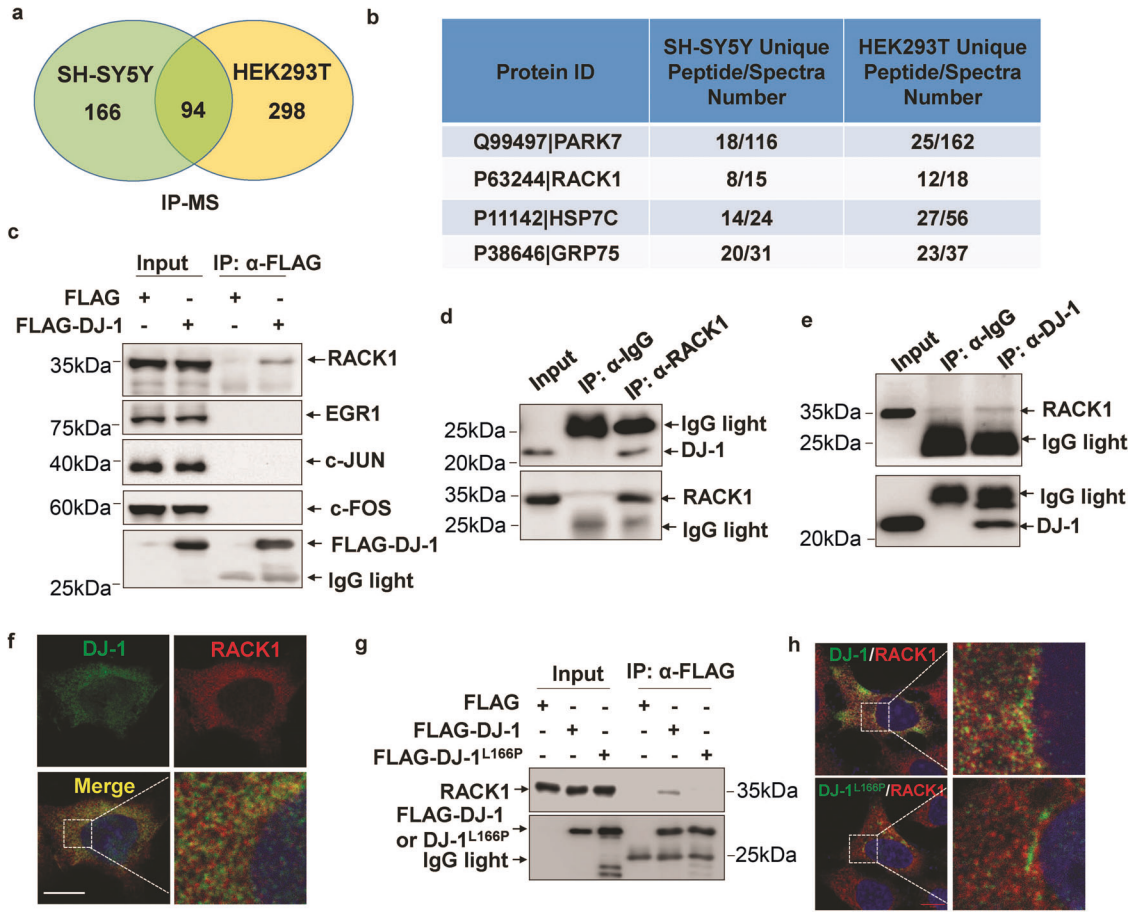

Protein ID	SH-SY5Y Unique Peptide/Spectra Number	HEK293T Unique Peptide/Spectra Number
Q99497|PARK7	18/116	25/162
P63244|RACK1	8/15	12/18
P11142|HSP7C	14/24	27/56
P38646|GRP75	20/31	23/37

Fig. 6 DJ-1 interacts with RACK1. a SH-SY5Y and HEK293T cells were transfected with FLAG or FLAG-DJ-1. Forty-eight hours after transfection, the cell lysates were subjected to IP using an anti-FLAG antibody followed by MS to identify DJ-1-interacting proteins. The proteins that were specifically pulled down by FLAG-DJ-1 but not FLAG were counted. **b** Partial list of proteins in DJ-1 complexes that exist in both SH-SY5Y and HEK293T cells. **c** SH-SY5Y cells were transfected with FLAG or FLAG-DJ-1. Forty-eight hours after transfection, the cell lysates were subjected to IP experiments. **d** The cell lysates of SH-SY5Y cells were subjected to IP experiments using an anti-RACK1 (**d**) or anti-DJ-1 antibody (**e**). **f** HEK293 cells were subjected to immunofluorescence using anti-RACK1 (green) and anti-DJ-1 (red) antibodies followed by DAPI staining (blue). **g** HEK293 cells were transfected with FLAG, FLAG-DJ-1 or FLAG-DJ-1^{L166P}. Forty-eight hours after transfection, the cell lysates were subjected to IP experiments. **h** HEK293 cells transfected with DJ-1-MYC or DJ-1^{L166P}-MYC were subjected to immunofluorescence using anti-RACK1 (red) and anti-MYC (green) antibodies followed by DAPI staining (blue).

PKC activation contributes to MAO-B expression induced by DJ-1 deficiency

As RACK1 acts as a scaffolding protein for PKC activation [50–52], we next investigated whether the binding of DJ-1 to RACK1 affects PKC activation. As shown in Fig. 7a, knockdown of DJ-1 significantly increased PKC phosphorylation. A previous study has suggested that a PKC agonist, phorbol 12-myristate 13-acetate (PMA), induces MAO-B but not MAO-A expression by activating the PKC/MAPKs/EGR1 signaling pathway [37]. Consistent with these findings, we also found that EGR1 expression was quickly induced by PMA. In addition, MAO-B rather than MAO-A expression was induced following EGR1 upregulation (Fig. 7b and c). We next investigated whether DJ-1 deficiency sensitized cells to MAO-B induction in response to PMA treatment. As shown in Fig. 7d and e, knockdown of DJ-1 increased MAO-B expression, and this effect was further aggravated after PMA treatment. We then investigated whether inhibition of PKC activity alleviated DJ-1 deficiency-mediated MAO-B expression. Treatment with sotrastaurin, a PKC inhibitor, largely restricted MAO-B expression induced by DJ-1 deficiency in cells (Fig. 7f and g). Together, these results suggest that DJ-1 represses MAO-B expression by interacting with RACK1 and inhibiting PKC/JNK signaling.

Inhibition of MAO-B activity prevents the sensitization to neuronal damage caused by DJ-1 deficiency

MAO-B contributes to neuronal damage by mediating DA degradation, which results in mitochondrial dysfunction and ROS production. Therefore, we next measured whether MAO-B induction by DJ-1 deficiency causes sensitization to neuronal damage and mitochondrial ROS production. Knockdown of DJ-1 alone induced slight cleavage of poly-ADP-ribose polymerase 1 (PARP-1) and caspase-3 and weak accumulation of mitochondrial ROS in cultured cells (Fig. 8a–c). Under DA treatment, knockdown of DJ-1 resulted in dramatic cleavage of PARP-1 and caspase-3 as well as large-scale accumulation of mitochondrial ROS (Fig. 8b and c). Interestingly, a MAO-B-specific inhibitor, Rasa, significantly alleviated the cleavage of PARP-1 and caspase-3 caused by DJ-1 knockdown in response to DA treatment (Fig. 8b). Rasa completely eliminated the increases in mitochondrial ROS levels caused by DJ-1 deficiency (Fig. 8c). In addition, compared with the control condition, DJ-1 deficiency led to a dramatic reduction in cell viability, especially in response to DA treatment, and Rasa eliminated the decline in cell viability caused by DJ-1 knockdown under DA treatment (Fig. 8d). MPTP, the best-known PD neurotoxic agent, exerts its specific toxicity on DA neurons upon conversion into MPP^+ through MAO-B. Therefore, we further

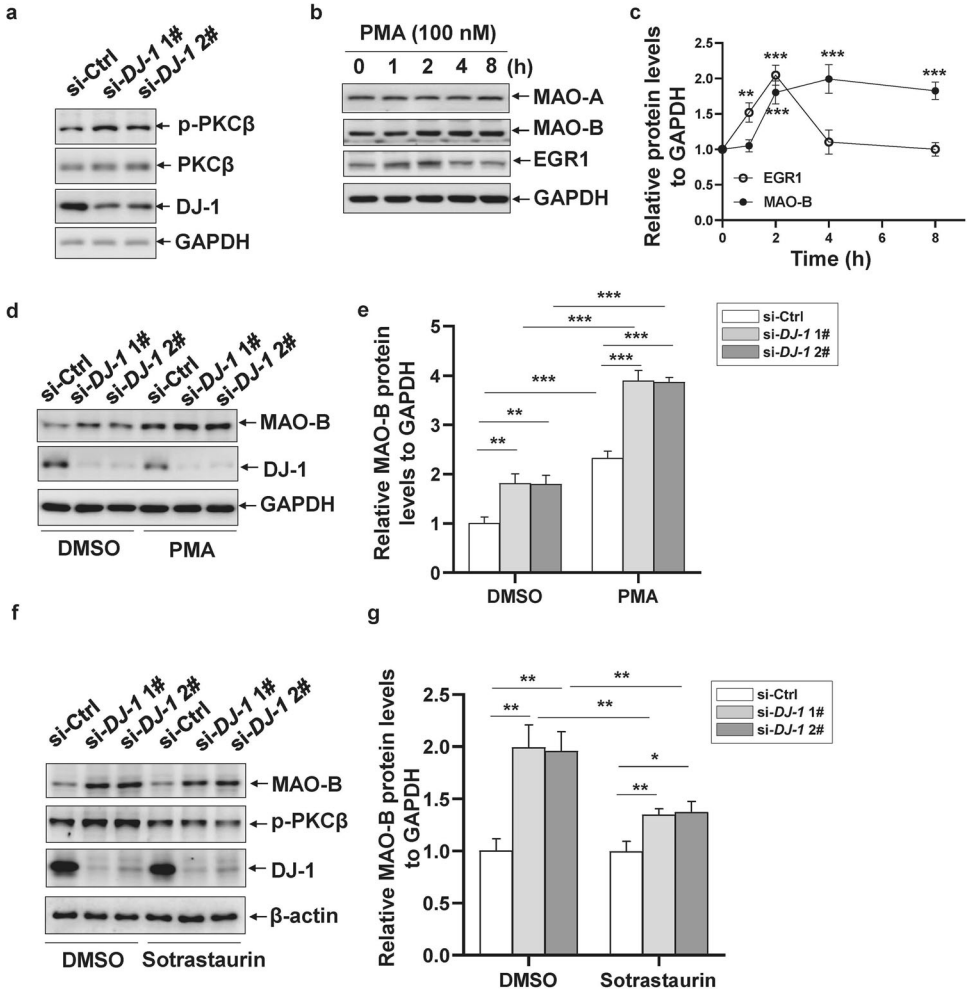

Fig. 7 PKC activation contributes to MAO-B expression by DJ-1 deficiency. a N2a cells were transfected with the indicated siRNAs. Seventy-two hours after transfection, the cell lysates were subjected to immunoblot analysis. **b** N2a cells were treated with 100 nM PMA for the indicated times, and then the cell lysates were subjected to immunoblot analysis. **c** The relative protein levels of MAO-B or EGR1 to GAPDH compared to those without PMA treatment in (**b**) were analyzed. **, $P < 0.01$, ***, $P < 0.001$, $n = 3$. **d** N2a cells were transfected with the indicated siRNAs. Seventy-two hours after transfection, cells were treated with 100 nM PMA for 4 h, and then the cell lysates were subjected to immunoblot analysis. **e** The relative protein levels of MAO-B to GAPDH in (**d**) were analyzed. **, $P < 0.01$, ***, $P < 0.001$, $n = 3$. **f** N2a cells were transfected with the indicated siRNAs. Twenty-four hours after transfection, cells were treated with 300 nM sotrastaurin for 48 h, and then the cell lysates were subjected to immunoblot analysis. **g** The relative protein levels of MAO-B to GAPDH in (**f**) were analyzed. *, $P < 0.05$, **, $P < 0.01$, $n = 3$.

investigated whether MAO-B expression induced by loss of DJ-1 contributes to MPTP-induced injury of DA neurons in vivo using *DJ-1*-KO mice and age-matched wild-type mice (Fig. 8e). As shown in Fig. 8f and g, although there was no significant difference in the number of TH-positive neurons between *DJ-1* wild-type and KO mice under physiological conditions, MPTP treatment dramatically reduced the number of TH-positive neurons in the SNs of *DJ-1*-KO mice compared with wild-type controls. Interestingly, treatment with Rasa significantly attenuated TH neuron loss in both *DJ-1* wild-type and KO mice, but especially in *DJ-1*-KO mice, in which the number of DA neurons was restored to a similar extent as that in wild-type mice (Fig. 8f and g). Similarly, Rasa treatment almost completely reversed the caspase-3 activation induced by *DJ-1* KO following MPTP administration (Fig. 8h). We also found that the TH protein levels were dramatically reduced in the SNs of *DJ-1*-KO mice treated with MPTP compared with those of the wild-type controls (Fig. 8h). However, Rasa treatment could not completely restore the TH protein levels in *DJ-1*-KO mice to wild-type levels (Fig. 8h), possibly because of the regulation of TH expression by DJ-1 [15–18]. Furthermore, the decrease in DA levels caused by *DJ-1* KO was further aggravated by MPTP treatment, and Rasa administration significantly restored DA levels (Fig. 8i). Although *DJ-1*-KO mice did not show severe motor dysfunction under normal conditions, *DJ-1*-KO mice showed a significant decrease in motor ability compared with that in wild-type mice in response to MPTP treatment; however, MAO-B inhibition by Rasa significantly attenuated the decline in motor ability caused by DJ-1 deficiency (Fig. 8j and k). Together, these results suggest that MAO-B expression activated by DJ-1 deficiency promotes DA degradation and DA neuronal damage in vitro and in vivo.

DISCUSSION

MAO-B plays an essential role in PD pathogenesis and is also a powerful therapeutic target of PD. Clinically, MAO-B inhibitors such as selegiline and Rasa are commonly used as adjuncts with *L*-DOPA or as monotherapies for PD treatment [54]. Increased expression and activity of MAO-B, but not MAO-A, is found in aging brains and PD brains [24, 25, 55, 56]. Upregulated expression or activity of MAO-B not only contributes to DA decline but also leads to excessive ROS production [24, 57, 58]. DA degradation occurs in both glial cells and DA neurons, in which

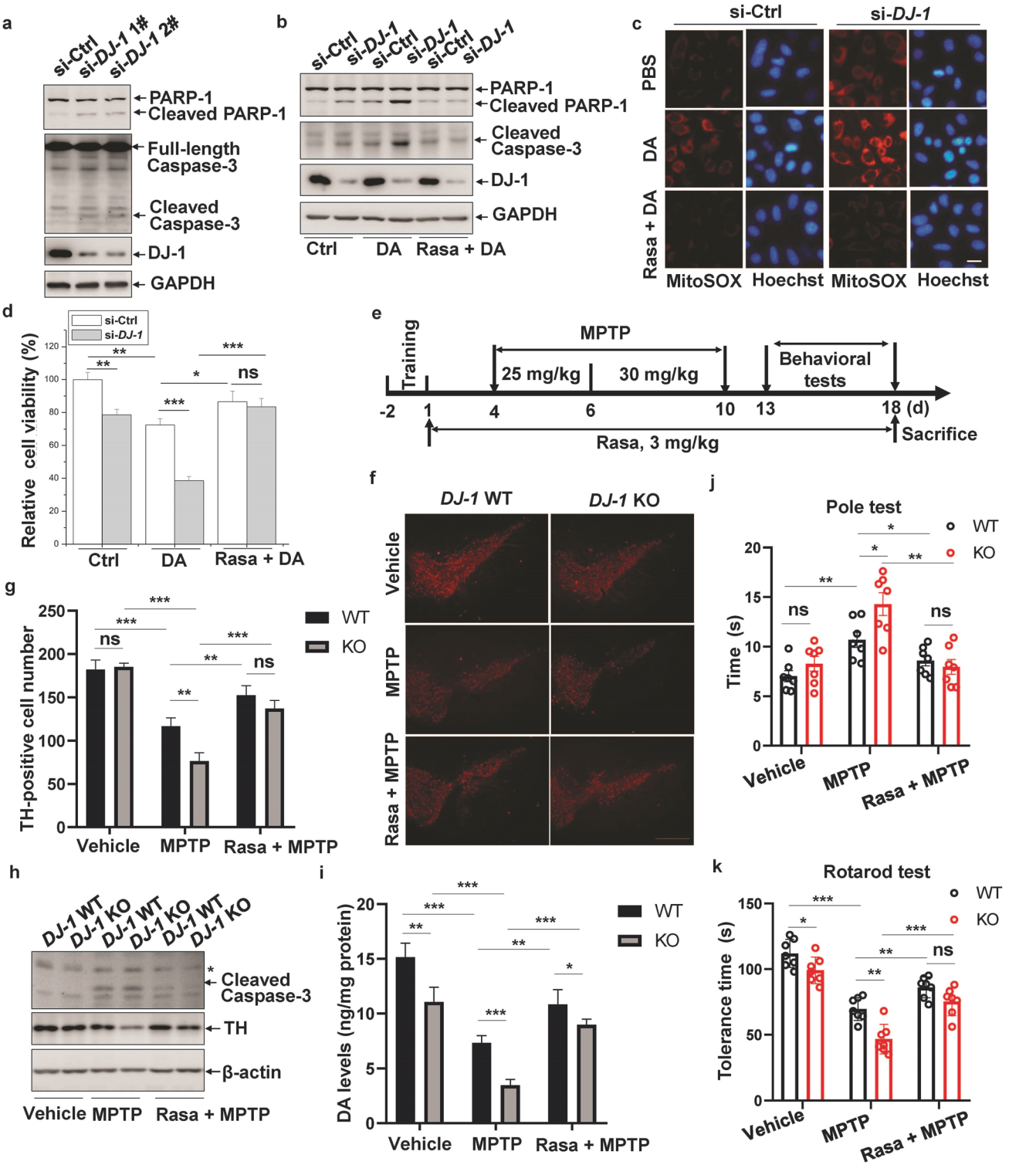

Fig. 8 Inhibition of MAO-B activity prevents the sensitization to neuronal damage caused by DJ-1 deficiency. a N2a cells were transfected with the indicated siRNAs. Seventy-two hours after transfection, the cell lysates were subjected to immunoblot analysis. **b**, **c** SH-SY5Y cells were transfected with the indicated siRNAs. Twenty-four hours after transfection, cells were pretreated with or without 2 nM Rasa for 24 h and then treated with 200 μM DA for another 24 h. Then, the cell lysates were subjected to immunoblot analysis (**b**), or the cells were stained with MitoSOX and Hoechst 33258. Bar, 10 μm (**c**). **d** The cells were treated as in (**b**), and the cells were subjected to the MTT assay. **e** Schematic diagram of drug administration in wild-type and *DJ-1*-KO mice. **f** WT and *DJ-1*-KO mice were subjected to drug administration as indicated, and then SN regions of slices were stained using an anti-TH antibody. Bar, 200 μm. **g** The number of TH-positive neurons in the SN of each slice was quantified. $^{**}P < 0.01$, $^{***}P < 0.001$, ns, no statistical significance, $n = 4$. **h** TH and the cleaved caspase-3 protein levels in the SN of mice were subjected to immunoblot analysis. *, unspecific bands. **i** DA levels in the mouse stratum were measured by HPLC. $^{*}P < 0.05$, $^{**}P < 0.01$, $^{***}P < 0.001$, $n = 4$. **j**, **k** Mice were subjected to the pole test (**j**) and rotarod test (**k**) every day from Day 13, and the climbing time and tolerance time were analyzed, respectively. $^{*}P < 0.05$, $^{**}P < 0.01$, $^{***}P < 0.001$, ns, no statistical significance, $n = 7$.

MAOs oxidize DA to form 3,4-dihydroxyphenylacetaldehyde (DOPAL) and hydrogen peroxide (H_2O_2) as byproducts in DA oxidative metabolism [19–21]. DOPAL can induce the opening of the mitochondrial permeability transition pore, thus triggering cell death [59]. As H_2O_2 is a natural byproduct of cellular metabolism, balance of H_2O_2 generation and elimination is essential for many physiological processes, but the amount of H_2O_2 produced during MAO activation can be increased 100-fold, thus leading to excessive ROS levels [60]. In addition to causing iron enrichment in the SNpc, H_2O_2 and iron generate highly reactive and destructive hydroxyl radicals to damage DA neurons via the Fenton reaction [61, 62]. Moreover, a recent study has suggested that MAO-B can drive NLRP3 inflammasome activation [63], which plays an essential role in PD neuropathology. Therefore, elucidating the regulatory mechanisms of PD genetic factors on MAO-B is of great significance for understanding the pathogenesis of PD and improving intervention strategies.

Mutations including L166P or deletions of DJ-1 are associated with an early-onset form of familial PD [64]. DJ-1 plays remarkable roles in mitochondrial function and antioxidant effects, and overexpression of DJ-1 can protect cells against DA- or MPTP-induced neurotoxicity and oxidative stress, while deletion of DJ-1 results in the opposite effect [65, 66]. However, the molecular mechanisms by which DJ-1 protects against the neurotoxicity of these agents and restricts mitochondrial ROS production are not fully understood. In the present study, we demonstrated that loss of function of DJ-1, a PD genetic factor, specifically activates the expression of MAO-B but not MAO-A, which contributes to DA metabolic dysfunction, mitochondrial oxidative stress and DA neurodegeneration. Mechanistically, wild-type DJ-1 rather than mutant DJ-1 interacts with RACK1 in the cytoplasm to inhibit PKC activity, thereby limiting the activation of JNK/AP-1 signaling and ultimately inhibiting EGR1/MAO-B expression. In addition, the MAO-B inhibitor Rasa can block *DJ-1* deletion-induced mitochondrial ROS accumulation and neuronal damage in response to neurotoxic stimuli in vitro or in vivo. Interestingly, in addition to our present findings that Rasa can attenuate neuronal damage caused by loss of DJ-1, previous findings have revealed that Rasa can reduce the microglia-mediated neurotoxicity induced by DJ-1 deficiency [67]. In addition to *PARK7/DJ-1*, other PD-associated genetic factors, including *SCNA* and *PRKN*, have been shown to regulate the expression or activity of MAO-B, which participates in PD pathogenesis. Parkin also inhibits the mRNA and protein expression of MAO-B, and elevated MAO-B levels decrease the ability of Parkin to clear damaged mitochondria [68, 69]. α-Synuclein directly binds to MAO-B rather than MAO-A and stimulates its enzymatic activity in DA neurons, leading to DA neurodegeneration [26]. These results indicate that elevation of MAO-B expression or activity is a common underlying pathway in PD pathogenesis.

In our study, EGR1 induction was responsible for the loss of DJ-1 or L166P mutant-induced MAO-B expression. Previous findings [37–39] and our results suggest that EGR1 is a specific transcription factor for the expression of MAO-B but not MAO-A. EGR1 induction has been observed in an acute MPTP model of PD [70]. Interestingly, EGR1 can also promote neuronal apoptosis by transactivating BIM expression [71]. Whether EGR1-mediated BIM expression contributes to the DJ-1 knockdown-induced slight cleavage of caspase-3 and PARP-1 is unclear. In addition to neurons, a recent study also indicated that early activation of EGR1 in astrocytes promotes neuroinflammation and contributes to DA neurodegeneration in MPTP-induced PD models [72]. DJ-1 has been demonstrated to influence the activity of JNK and ERK1/2, whose pathways are crucial for EGR1 expression [43–46, 73]. We further demonstrated that JNK/c-JUN cascade activation but not ERK1/2 activity is involved in DJ-1 deficiency-induced EGR1 and MAO-B expression. The JNK inhibitor SP600125 completely blocked DJ-1 deficiency-induced EGR1 and MAO-B expression. JNK activation has been found to occur in various types of PD cellular and animal models [74]. Our previous study illustrated that loss of DJ-1 activates the JNK/Beclin1 pathway to regulate autophagy in cancer cells [75].

RACK1, a conserved scaffolding protein, interacts with multiple signaling proteins via its seven-repeat WD domains. PKC is the most studied binding partner of RACK1, and RACK1 stabilizes the active conformation of PKC [76]. PKC-mediated activation of JNK/AP-1/EGR1 cascades is responsible for MAO-B induction [37]. Interestingly, we found that wild-type DJ-1 binds to RACK1 in the cytoplasm through IP-MS and subsequent validation. The L166P mutation results in localization mainly in mitochondria, not in the

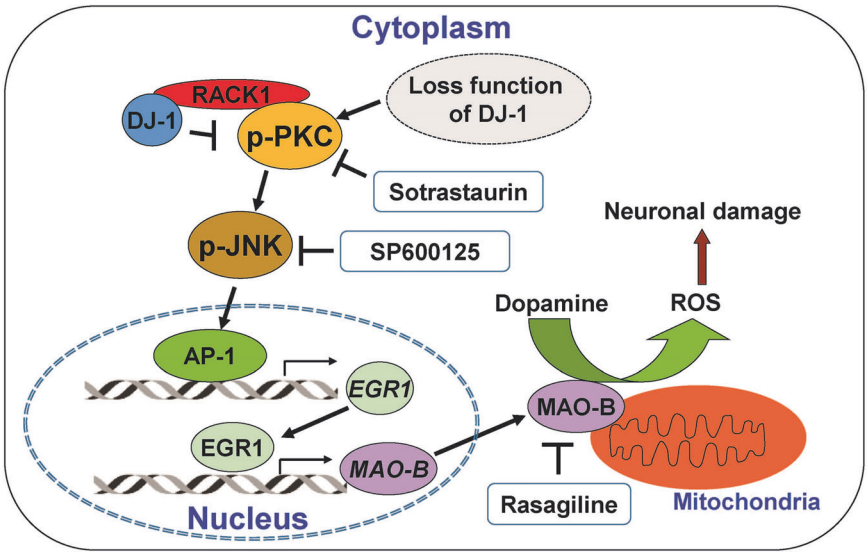

Fig. 9 Schematic diagram of the mechanism by which DJ-1 regulates MAO-B expression. Wild-type DJ-1 binds to RACK1 and inhibits the activity of PKC, which represses full JNK activation and AP-1 transcriptional activity, thus inhibiting EGR1 and MAO-B expression. DJ-1 deficiency or mutations lead to PKC/JNK/AP-1 cascade activation and EGR1/MAO-B expression, mitochondrial ROS production, and DA neuronal damage. The PKC inhibitor sotrastaurin or the JNK inhibitor SP600125 can inhibit EGR1 and MAO-B expression and alleviate DA neuronal damage caused by loss of DJ-1 function. In addition, the MAO-B inhibitor rasagiline can prevent DA degradation and ROS-mediated neuronal damage caused by loss of DJ-1.

cytoplasm or nucleus [10, 29], which may explain why the mutant cannot bind to RACK1. A previous study has indicated that the association between DJ-1 and RACK1 influences RACK1 stability and protects neurons from H_2O_2- or MPP^+-induced apoptosis [77]. However, we did not observe that silencing DJ-1 affected the protein levels of RACK1. In the present study, we found that DJ-1 binds to RACK1 and that loss of DJ-1 leads to PKC activation. Changes in PKC have already been described in the pathogenesis of PD models. PKCβ-mediated p66shc phosphorylation is indispensable for the cytotoxicity of 6-OHDA, and its inhibitor suppresses 6-OHDA-induced neurotoxicity [78]. PKC activation initiates DA neuronal ferroptosis, a newly characterized form of cell death linked to oxidative stress, and PKC inhibitors are strong drug candidates to pharmacologically modulate the ferroptotic signaling cascade in PD [79, 80]. PKC activation induced by DJ-1 deletion may contribute to full JNK activation, as the PKC inhibitor could not completely block the expression of MAO-B induced by DJ-1 deletion, while the JNK inhibitor could (Fig. 5c and 7f). Indeed, RACK1/PKC-augmented JNK activation is required for MAPK kinase 4/7 (MKK4/7) [51, 52]. MEKK1 and its downstream protein MKK4/7 may also contribute to JNK activation induced by DJ-1 deficiency, since DJ-1 has been reported to bind to MAPK kinase kinase 1 (MEKK1) and inhibit activation of the MEKK1/MKK/JNK pathway [81].

In conclusion, our data demonstrate the mechanism of DJ-1 in MAO-B expression, which involves interaction of DJ-1 with RACK1 and regulation of PKC/JNK pathway activity. Loss of DJ-1 leads to PKC activation, which contributes to full JNK activation, activates AP-1 transcriptional activity, and subsequently promotes *EGR1* transcription. Upon its increase in expression, EGR1 transcriptionally activates the expression of MAO-B, which localizes at mitochondria and mediates DA degradation, leading to excess ROS production and damaging DA neurons (Fig. 9). The finding that RACK1/PKC signaling is involved in the regulation of MAO-B expression by DJ-1 may be helpful for understanding PD pathogenesis.

DATA AVAILABILITY

The data supporting the findings in this study are available within the paper. Other transcriptome sequencing and mass spectrometry data supporting the findings of this study are available from the corresponding author on reasonable request.

AUTHOR CONTRIBUTIONS

HGR and BL designed the study. LLL, YH, and ZJZ performed most of the experiments. YQW, YWH, and BL performed some of the biochemical and cellular experiments. EK, JQD, and DKG analyzed the data. HGR drafted the paper. BL and GHW revised the paper. All authors read and approved the paper.

FUNDING

This work was supported by the National Natural Science Foundation of China (Nos. 32170987, 31970966 and 32261133525), the Russian Science Foundation (No. 23-44-00054), the Natural Science Foundation of Jiangsu Province (BK20200213) and a Project Funded by the Priority Academic Program Development of Jiangsu Higher Education Institutions.

ADDITIONAL INFORMATION

Competing interests: The authors declare no competing interests.

REFERENCES

1. Kalia LV, Lang AE. Parkinson's disease. Lancet. 2015;386:896–912.
2. Bloem BR, Okun MS, Klein C. Parkinson's disease. Lancet. 2021;397:2284–303.
3. Liu Y, Niu L, Liu X, Cheng C, Le W. Recent progress in non-motor features of Parkinson's disease with a focus on circadian rhythm dysregulation. Neurosci Bull. 2021;37:1010–24.
4. Armstrong MJ, Okun MS. Diagnosis and treatment of Parkinson disease: a review. JAMA. 2020;323:548–60.
5. Li S, Jia C, Li T, Le W. Hot topics in recent Parkinson's disease research: where we are and where we should go. Neurosci Bull. 2021;37:1735–44.
6. Mao Q, Qin WZ, Zhang A, Ye N. Recent advances in dopaminergic strategies for the treatment of Parkinson's disease. Acta Pharmacol Sin. 2020;41:471–82.
7. Trist BG, Hare DJ, Double KL. Oxidative stress in the aging substantia nigra and the etiology of Parkinson's disease. Aging Cell. 2019;18:e13031.
8. Dauer W, Przedborski S. Parkinson's disease: mechanisms and models. Neuron. 2003;39:889–909.
9. Malpartida AB, Williamson M, Narendra DP, Wade-Martins R, Ryan BJ. Mitochondrial dysfunction and mitophagy in Parkinson's disease: from mechanism to therapy. Trends Biochem Sci. 2021;46:329–43.
10. Bonifati V, Rizzu P, van Baren MJ, Schaap O, Breedveld GJ, Krieger E, et al. Mutations in the DJ-1 gene associated with autosomal recessive early-onset parkinsonism. Science. 2003;299:256–9.
11. Kumaran R, Vandrovcova J, Luk C, Sharma S, Renton A, Wood NW, et al. Differential DJ-1 gene expression in Parkinson's disease. Neurobiol Dis. 2009;36:393–400.
12. Neves M, Graos M, Anjo SI, Manadas B. Modulation of signaling pathways by DJ-1: An updated overview. Redox Biol. 2022;51:102283.
13. Dekker M, Bonifati V, van Swieten J, Leenders N, Galjaard RJ, Snijders P, et al. Clinical features and neuroimaging of PARK7-linked parkinsonism. Mov Disord. 2003;18:751–7.
14. Dekker MC, Eshuis SA, Maguire RP, Veenma-van der Duijn L, Pruim J, Snijders PJ, et al. PET neuroimaging and mutations in the DJ-1 gene. J Neural Transm (Vienna). 2004;111:1575–81.
15. Xu X, Wang R, Hao Z, Wang G, Mu C, Ding J, et al. DJ-1 regulates tyrosine hydroxylase expression through CaMKKbeta/CaMKIV/CREB1 pathway in vitro and in vivo. J Cell Physiol. 2020;235:869–79.
16. Lu L, Sun X, Liu Y, Zhao H, Zhao S, Yang H. DJ-1 upregulates tyrosine hydroxylase gene expression by activating its transcriptional factor Nurr1 via the ERK1/2 pathway. Int J Biochem Cell Biol. 2012;44:65–71.
17. Ishikawa S, Taira T, Takahashi-Niki K, Niki T, Ariga H, Iguchi-Ariga SM. Human DJ-1-specific transcriptional activation of tyrosine hydroxylase gene. J Biol Chem. 2010;285:39718–31.
18. Zhong N, Kim CY, Rizzu P, Geula C, Porter DR, Pothos EN, et al. DJ-1 transcriptionally up-regulates the human tyrosine hydroxylase by inhibiting the sumoylation of pyrimidine tract-binding protein-associated splicing factor. J Biol Chem. 2006;281:20940–8.
19. Burbulla LF, Song P, Mazzulli JR, Zampese E, Wong YC, Jeon S, et al. Dopamine oxidation mediates mitochondrial and lysosomal dysfunction in Parkinson's disease. Science. 2017;357:1255–61.
20. Masato A, Plotegher N, Boassa D, Bubacco L. Impaired dopamine metabolism in Parkinson's disease pathogenesis. Mol Neurodegener. 2019;14:35.
21. Juarez Olguin H, Calderon Guzman D, Hernandez Garcia E, Barragan Mejia G. The role of dopamine and its dysfunction as a consequence of oxidative stress. Oxid Med Cell Longev. 2016;2016:9730467.
22. Naoi M, Maruyama W, Inaba-Hasegawa K. Type A and B monoamine oxidase in age-related neurodegenerative disorders: their distinct roles in neuronal death and survival. Curr Top Med Chem. 2012;12:2177–88.
23. Tipton KF, Boyce S, O'Sullivan J, Davey GP, Healy J. Monoamine oxidases: certainties and uncertainties. Curr Med Chem. 2004;11:1965–82.
24. Youdim MB, Edmondson D, Tipton KF. The therapeutic potential of monoamine oxidase inhibitors. Nat Rev Neurosci. 2006;7:295–309.
25. Damier P, Kastner A, Agid Y, Hirsch EC. Does monoamine oxidase type B play a role in dopaminergic nerve cell death in Parkinson's disease? Neurology. 1996;46:1262–9.
26. Kang SS, Ahn EH, Zhang Z, Liu X, Manfredsson FP, Sandoval IM, et al. alpha-Synuclein stimulation of monoamine oxidase-B and legumain protease mediates the pathology of Parkinson's disease. EMBO J. 2018;37:e98878.
27. Goldberg MS, Pisani A, Haburcak M, Vortherms TA, Kitada T, Costa C, et al. Nigrostriatal dopaminergic deficits and hypokinesia caused by inactivation of the familial Parkinsonism-linked gene DJ-1. Neuron. 2005;45:489–96.
28. Ren H, Fu K, Wang D, Mu C, Wang G. Oxidized DJ-1 interacts with the mitochondrial protein BCL-XL. J Biol Chem. 2011;286:35308–17.
29. Ren H, Fu K, Mu C, Zhen X, Wang G. L166P mutant DJ-1 promotes cell death by dissociating Bax from mitochondrial Bcl-X_L. Mol Neurodegener. 2012;7:40.
30. Clarke N, Arenzana N, Hai T, Minden A, Prywes R. Epidermal growth factor induction of the c-jun promoter by a Rac pathway. Mol Cell Biol. 1998;18:1065–73.
31. Vasanwala FH, Kusam S, Toney LM, Dent AL. Repression of AP-1 function: a mechanism for the regulation of Blimp-1 expression and B lymphocyte differentiation by the B cell lymphoma-6 protooncogene. J Immunol. 2002;169:1922–9.
32. Xia Q, Hu Q, Wang H, Yang H, Gao F, Ren H, et al. Induction of COX-2-PGE2 synthesis by activation of the MAPK/ERK pathway contributes to neuronal death triggered by TDP-43-depleted microglia. Cell Death Dis. 2015;6:e1702.

33. Guo DK, Zhu Y, Sun HY, Xu XY, Zhang S, Hao ZB, et al. Pharmacological activation of REV-ERBalpha represses LPS-induced microglial activation through the NF-kappaB pathway. Acta Pharmacol Sin. 2019;40:26–34.
34. Sun HY, Wu J, Wang R, Zhang S, Xu H, Kaznacheyeva E, et al. Pazopanib alleviates neuroinflammation and protects dopaminergic neurons in LPS-stimulated mouse model by inhibiting MEK4-JNK-AP-1 pathway. Acta Pharmacol Sin. 2022. https://doi.org/10.1038/s41401-022-01030-1. Online ahead of print.
35. Gonzalez-Lopez E, Vrana KE. Dopamine beta-hydroxylase and its genetic variants in human health and disease. J Neurochem. 2020;152:157–81.
36. Shih JC, Wu JB, Chen K. Transcriptional regulation and multiple functions of MAO genes. J Neural Transm (Vienna). 2011;118:979–86.
37. Wong WK, Ou XM, Chen K, Shih JC. Activation of human monoamine oxidase B gene expression by a protein kinase C MAPK signal transduction pathway involves c-Jun and Egr-1. J Biol Chem. 2002;277:22222–30.
38. Arige V, Agarwal A, Khan AA, Kalyani A, Natarajan B, Gupta V, et al. Regulation of monoamine oxidase B gene expression: key roles for transcription factors Sp1, Egr1 and CREB, and microRNAs miR-300 and miR-1224. J Mol Biol. 2019;431:1127–47.
39. Shih JC, Chen K. Regulation of MAO-A and MAO-B gene expression. Curr Med Chem. 2004;11:1995–2005.
40. Hijioka M, Inden M, Yanagisawa D, Kitamura Y. DJ-1/PARK7: A new therapeutic target for neurodegenerative disorders. Biol Pharm Bull. 2017;40:548–52.
41. Ou XM, Chen K, Shih JC. Dual functions of transcription factors, transforming growth factor-beta-inducible early gene (TIEG)2 and Sp3, are mediated by CACCC element and Sp1 sites of human monoamine oxidase (MAO) B gene. J Biol Chem. 2004;279:21021–8.
42. Grunewald M, Johnson S, Lu D, Wang Z, Lomberk G, Albert PR, et al. Mechanistic role for a novel glucocorticoid-KLF11 (TIEG2) protein pathway in stress-induced monoamine oxidase A expression. J Biol Chem. 2012;287:24195–206.
43. Hoffmann E, Ashouri J, Wolter S, Doerrie A, Dittrich-Breiholz O, Schneider H, et al. Transcriptional regulation of EGR-1 by the interleukin-1-JNK-MKK7-c-Jun pathway. J Biol Chem. 2008;283:12120–8.
44. Aggeli IK, Beis I, Gaitanaki C. ERKs and JNKs mediate hydrogen peroxide-induced Egr-1 expression and nuclear accumulation in H9c2 cells. Physiol Res. 2010;59:443–54.
45. Iyoda T, Zhang F, Sun L, Hao F, Schmitz-Peiffer C, Xu X, et al. Lysophosphatidic acid induces early growth response-1 (Egr-1) protein expression via protein kinase Cdelta-regulated extracellular signal-regulated kinase (ERK) and c-Jun N-terminal kinase (JNK) activation in vascular smooth muscle cells. J Biol Chem. 2012;287:22635–42.
46. Pagel JI, Deindl E. Disease progression mediated by egr-1 associated signaling in response to oxidative stress. Int J Mol Sci. 2012;13:13104–17.
47. Angel P, Hattori K, Smeal T, Karin M. The jun proto-oncogene is positively autoregulated by its product, Jun/AP-1. Cell. 1988;55:875–85.
48. Behrens A, Sibilia M, Wagner EF. Amino-terminal phosphorylation of c-Jun regulates stress-induced apoptosis and cellular proliferation. Nat Genet. 1999;21:326–9.
49. Kappelmann M, Bosserhoff A, Kuphal S. AP-1/c-Jun transcription factors: regulation and function in malignant melanoma. Eur J Cell Biol. 2014;93:76–81.
50. Li JJ, Xie D. RACK1, a versatile hub in cancer. Oncogene. 2015;34:1890–8.
51. Lopez-Bergami P, Ronai Z. Requirements for PKC-augmented JNK activation by MKK4/7. Int J Biochem Cell Biol. 2008;40:1055–64.
52. Lopez-Bergami P, Habelhah H, Bhoumik A, Zhang W, Wang LH, Ronai Z. RACK1 mediates activation of JNK by protein kinase C [corrected]. Mol Cell. 2005;19:309–20.
53. Miller DW, Ahmad R, Hague S, Baptista MJ, Canet-Aviles R, McLendon C, et al. L166P mutant DJ-1, causative for recessive Parkinson's disease, is degraded through the ubiquitin-proteasome system. J Biol Chem. 2003;278:36588–95.
54. Tan YY, Jenner P, Chen SD. Monoamine oxidase-B inhibitors for the treatment of Parkinson's disease: past, present, and future. J Parkinsons Dis. 2022;12:477–93.
55. Nicotra A, Pierucci F, Parvez H, Senatori O. Monoamine oxidase expression during development and aging. Neurotoxicology. 2004;25:155–65.
56. Li L, Zhang CW, Chen GY, Zhu B, Chai C, Xu QH, et al. A sensitive two-photon probe to selectively detect monoamine oxidase B activity in Parkinson's disease models. Nat Commun. 2014;5:3276.
57. Weng M, Xie X, Liu C, Lim KL, Zhang CW, Li L. The sources of reactive oxygen species and its possible role in the pathogenesis of Parkinson's disease. Parkinsons Dis. 2018;2018:9163040.
58. Saller S, Kunz L, Berg D, Berg U, Lara H, Urra J, et al. Dopamine in human follicular fluid is associated with cellular uptake and metabolism-dependent generation of reactive oxygen species in granulosa cells: implications for physiology and pathology. Hum Reprod. 2014;29:555–67.
59. Kristal BS, Conway AD, Brown AM, Jain JC, Ulluci PA, Li SW, et al. Selective dopaminergic vulnerability: 3,4-dihydroxyphenylacetaldehyde targets mitochondria. Free Radic Biol Med. 2001;30:924–31.
60. Cohen G, Kesler N. Monoamine oxidase and mitochondrial respiration. J Neurochem. 1999;73:2310–5.
61. Singh YP, Pandey A, Vishwakarma S, Modi G. A review on iron chelators as potential therapeutic agents for the treatment of Alzheimer's and Parkinson's diseases. Mol Divers. 2019;23:509–26.
62. Ben-Shachar D, Zuk R, Glinka Y. Dopamine neurotoxicity: inhibition of mitochondrial respiration. J Neurochem. 1995;64:718–23.
63. Sanchez-Rodriguez R, Munari F, Angioni R, Venegas F, Agnellini A, Castro-Gil MP, et al. Targeting monoamine oxidase to dampen NLRP3 inflammasome activation in inflammation. Cell Mol Immunol. 2021;18:1311–3.
64. da Costa CA. DJ-1: a newcomer in Parkinson's disease pathology. Curr Mol Med. 2007;7:650–7.
65. Lev N, Barhum Y, Pilosof NS, Ickowicz D, Cohen HY, Melamed E, et al. DJ-1 protects against dopamine toxicity: implications for Parkinson's disease and aging. J Gerontol A Biol Sci Med Sci. 2013;68:215–25.
66. Lev N, Ickowicz D, Barhum Y, Lev S, Melamed E, Offen D. DJ-1 protects against dopamine toxicity. J Neural Transm (Vienna). 2009;116:151–60.
67. Trudler D, Weinreb O, Mandel SA, Youdim MB, Frenkel D. DJ-1 deficiency triggers microglia sensitivity to dopamine toward a pro-inflammatory phenotype that is attenuated by rasagiline. J Neurochem. 2014;129:434–47.
68. Jiang HB, Jiang Q, Liu WH, Feng J. Parkin suppresses the expression of monoamine oxidases. J Biol Chem. 2006;281:8591–9.
69. Siddiqui A, Hanson I, Andersen JK. Mao-B elevation decreases parkin's ability to efficiently clear damaged mitochondria: protective effects of rapamycin. Free Radic Res. 2012;46:1011–8.
70. Smith TS, Trimmer PA, Khan SM, Tinklepaugh DL, Bennett JP Jr. Mitochondrial toxins in models of neurodegenerative diseases. II: Elevated zif268 transcription and independent temporal regulation of striatal D1 and D2 receptor mRNAs and D1 and D2 receptor-binding sites in C57BL/6 mice during MPTP treatment. Brain Res. 1997;765:189–97.
71. Xie B, Wang C, Zheng Z, Song B, Ma C, Thiel G, et al. Egr-1 transactivates Bim gene expression to promote neuronal apoptosis. J Neurosci. 2011;31:5032–44.
72. Yu Q, Huang Q, Du X, Xu S, Li M, Ma S. Early activation of Egr-1 promotes neuroinflammation and dopaminergic neurodegeneration in an experimental model of Parkinson's disease. Exp Neurol. 2018;302:145–54.
73. Cao J, Lou S, Ying M, Yang B. DJ-1 as a human oncogene and potential therapeutic target. Biochem Pharmacol. 2015;93:241–50.
74. Kim EK, Choi EJ. Compromised MAPK signaling in human diseases: an update. Arch Toxicol. 2015;89:867–82.
75. Ren H, Fu K, Mu C, Li B, Wang D, Wang G. DJ-1, a cancer and Parkinson's disease associated protein, regulates autophagy through JNK pathway in cancer cells. Cancer Lett. 2010;297:101–8.
76. Kershner L, Welshhans K. RACK1 regulates neural development. Neural Regen Res. 2017;12:1036–9.
77. Ma J, Wu R, Zhang Q, Wu JB, Lou J, Zheng Z, et al. DJ-1 interacts with RACK1 and protects neurons from oxidative-stress-induced apoptosis. Biochem J. 2014;462:489–97.
78. Yamamori T, Mizobata A, Saito Y, Urano Y, Inanami O, Irani K, et al. Phosphorylation of p66shc mediates 6-hydroxydopamine cytotoxicity. Free Radic Res. 2011;45:342–50.
79. Do Van B, Gouel F, Jonneaux A, Timmerman K, Gele P, Petrault M, et al. Ferroptosis, a newly characterized form of cell death in Parkinson's disease that is regulated by PKC. Neurobiol Dis. 2016;94:169–78.
80. Zhu HY, He QJ, Yang B, Cao J. Beyond iron deposition: making sense of the latest evidence on ferroptosis in Parkinson's disease. Acta Pharmacol Sin. 2021;42:1379–81.
81. Mo JS, Kim MY, Ann EJ, Hong JA, Park HS. DJ-1 modulates UV-induced oxidative stress signaling through the suppression of MEKK1 and cell death. Cell Death Differ. 2008;15:1030–41.